Device Modelling of MgO-Barrier Tunnelling Magnetoresistors for Hybrid Spintronic-CMOS

Siming Zuo, *Student Member, IEEE*, Kianoush Nazarpour, *Senior Member, IEEE,* and Hadi Heidari, *Senior Member, IEEE*

***Abstract*— Spintronic sensors, that are based on the tunnelling-magnetoresistive (TMR) effect, have been utilized in detecting low magnetic fields. However, still no computer-based model of these devices is available to integrated circuit designer to implement them in a hybrid spintronic-CMOS system. We developed a finite element method (FEM)-based model of a MgO-barrier TMR device in *COMSOL Multiphysics*®. The parameters of this model were extracted from the state-of-the-art fabrication and experimental data. Results were compared with respect to the model geometry and the used material. The proposed TMR sensor model offers a linear response with a high TMR ratio of 233% at 10 mV power supply. The model was exported to *Cadence*© *Spectre* to create a compact model using *Verilog-A* language. The developed sensor model was simulated with its analog front-end in same environment. This model provided a reliable benchmark for modelling of the future hybrid spintronic-CMOS developments.**

***Index Terms*— CMOS, COMSOL Multiphysics, Spintronics, Tunnelling Magnetoresistors, Verilog-A.**

I. Introduction

Spintronics device modelling, so far, has been focused on the development of memory elements in magnetoresistive random access memory to meet rapidly growing demands for storage capacity [1]. Recently, magnetoresistive (MR) sensors have attracted significant attention in medical applications; ranging from point-of-care diagnostics [2-5] to flexible and implantable magnetoelectronics [6-9]. Extensive research over the past decade in materials and physics [10] has promised to advance high-performance tunnelling magnetoresistance (TMR) effect in magnetic tunnel junctions (MTJs) devices [11], exhibiting a large MR effect at room temperature. This has resulted in TMR sensors that are of a lower profile, faster, more reliable, and cheaper than other magnetic sensors. With pico-Tesla field detectivity [12] and CMOS-compatible benefits [13, 14], the TMR sensor provides advantageous solutions to form a miniaturised system for various biomedical wearable and implantable technologies [15, 16].

One critical aspect in the design of the TMR sensors is that one should predict the effect of the materials and fabrication process on its behaviour within an external magnetic field. However, fabrication and testing of all combinations is time-consuming and expensive. Therefore, simulation techniques can be utilized to estimate the behavior of certain material combinations and sensor geometries. However, there is no reliable model of TMR sensors to export into circuit design environments, such as *Cadence*© *Spectre*.

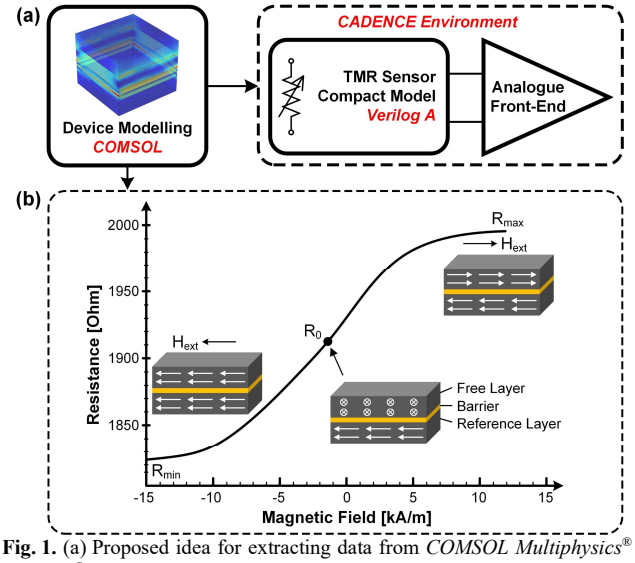

Fig. 1. (a) Proposed idea for extracting data from *COMSOL Multiphysics*® to *Cadence*© environment; (b) R(H) linear behavior and typical magnetization orientations correspondence of TMR sensor.

We developed a compact model of high-performance TMR sensors with the ultimate goal of miniaturizing them into the CMOS technology. Figure 1(a) illustrates the components of our design. A finite element method (FEM) model of a TMR device was created in *COMSOL Multiphysics*®. The parameters of this model were then exported into *Cadence* using *Verilog-A* language so that the model can be integrated into a standard CMOS-based analogue front-end (AFE) circuit with power management unit [17], to achieve on-chip signal processing and noise and offset cancellation.

II. TMR Structure and Modelling

The TMR effect is a nanoscale phenomenon in which, under the right conditions, electrons can tunnel through a very thin ordinary insulating material. Figure 1(b) shows the basic structure consisting of free layer/barrier/pinned layers, and its transfer curve. When a bias voltage is applied to the TMR sensor, it may exhibit electrical conducting properties and its electrical resistance varies as a linear function of the magnetic field strength over a certain field range. This occurs due to the dependence of the tunnelling probability on the relative orientation of the magnetization in the two ferromagnetic (FM)

This work was supported by the Royal Society under grant "MAGLAB" RSG\R1\180269". The work of KN is supported by grants EP/N023080/1 and EP/R004242/1 from EPSRC, UK.

S. Zuo and H. Heidari are with Microelectronics Lab (meLAB), School of Engineering at University of Glasgow, G12 8QQ, United Kingdom. (e-mail: z.siming.1@research.gla.ac.uk and Hadi.Heidari@glasgow.ac.uk).

K. Nazarpour is School of Engineering, and Institute of Neuroscience, Newcastle University, NE1 7RU, United Kingdom.

layers. The largest (R_{AP}) and lowest (R_P) resistance values are obtained when the FM layers have antiparallel and parallel orientations respectively. The TMR is defined as the ratio [18]:

$$TMR = \frac{R_{AP} - R_P}{R_P} \quad (1)$$

For an ideal magnetic sensor, the transfer curve is linear and hysteresis-free within the intended field operating range. The curve possesses two stable resistance plateaus and a linear reversible path between them. Saturation fields (H_{sat}) define the ideal linear range ($2H_{sat}$) of the device, where a dR variation corresponds to a single dH value. The key feature of a magnetic sensor response is its field sensitivity (S), which represents how reactive a sensor is to a field variation. This can be measured experimentally from the slope of the transfer curve, and commonly, the sensitivity is normalized as the following

$$S = \frac{1}{R_{min}}\left(\frac{\Delta R}{\Delta H}\right)_{linear} = \frac{TMR}{(\Delta H)_{linear}}. \quad (2)$$

It is noted that the high sensitivity of TMR sensor is obtained from higher TMR ratio and smaller linear magnetic field range, while the linear range depends on the material and geometry (shape and dimensions) of the device; while the TMR is intrinsic to the FM/barrier/FM structure and its interfaces [19]. To achieve the linear behavior, shown in Fig. 1(b), free and pinned layer magnetizations are set orthogonal to each other and the external magnetic field is applied perpendicular to the free layer but parallel to the pinned one.

Numerical simulation was performed using FEM with *COMSOL Multiphysics*®. In addition, the structure was divided into several elements, and then reconnected, resulting in a set of simultaneous algebraic equations with finite degrees of freedom. Previous FEM simulations of TMR biosensors are summarized in [20]. Figure 2(a) shows the simulation details. The proposed TMR structure is a MTJ multilayer between two leads in a current-perpendicular-to-plane geometry. This is a complex stack with double-exchange electrodes, consisting of bottom lead, bottom antiferromagnet (AFM), pinned layer (PL), spacer, reference layer (RL), barrier, sensing layer (SL), top-antiferromagnet, and top-lead. To increase the exchange field and make the MTJ more thermally stable, a synthetic antiferromagnetic (SAF) structure was used instead of a single FM in the pinned layer adjacent to the AFM. The SAF structure consists of two or more FM layers separated by thin Ru layers [21], coupled by RKKY theory [22]. In addition, the method of fixing the magnetization of the pinned layer at a defined direction is exchange coupling between the FM and AFM layer. Only magnetic fields above the exchange field can reverse the pinned layer magnetization. The arrows in Fig. 2(a) indicate directions of magnetization and the applied magnetic field. Finally, to mimic the experimental conditions, thick and low resistivity top and bottom electrodes were considered and subjected to a bias voltage of 10 mV.

The used materials and their properties, such as electrical conductivity, coercivity, relative permeability, and relative permittivity were modelled and simulated by imported

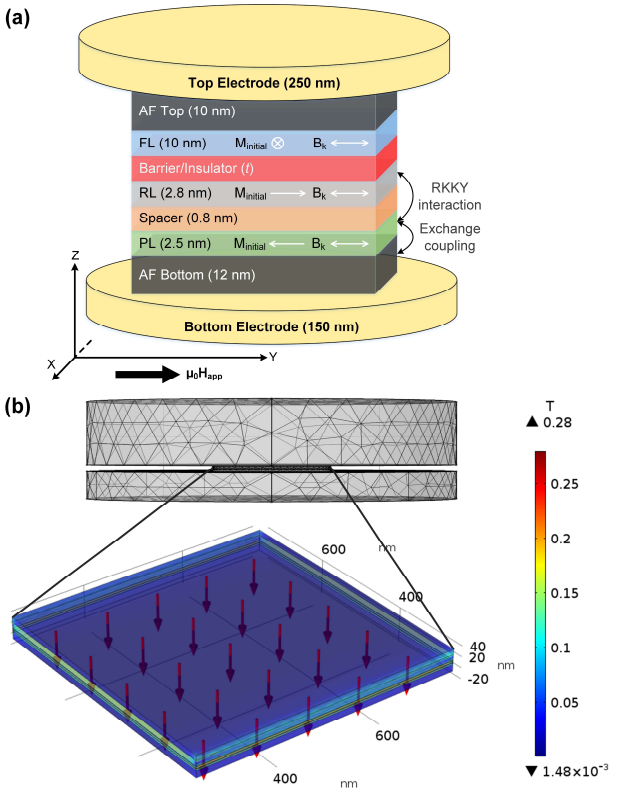

Fig. 2. (a) Schematic of the MTJ stack layout used for FEM simulations and orientation of simulation input vectors relative to coordinate axes. (b) Mesh created in COMSOL software and then zooming in on the MTJ.

parameters from state-of-the-art fabrication and experimental data [23, 24]. Input parameters for the simulations are summarized in Table I: saturation magnetization (M_s), exchange length (l_{ex}) and induced anisotropy field (B_k).

Furthermore, in this study, the geometry of the MTJ was defined as a tetrahedral mesh of user-defined size, dividing the 3D structures into small elements. This was used to estimate the current distribution in the MTJ devices with different strength of the magnetic field and also to account for possible geometrical mismatches. The computational mesh and an enlarged view of the thin film structure (1 μm × 1 μm in length and width) on the MTJ are demonstrated in Fig. 2(b), resulting in a system of ~10^8 tetrahedral finite element with an average element size of 10 nm in the top and bottom leads, 1 nm in the FL and AMF layers, and 0.1 nm in the remaining layers. The mesh resolutions are very fine to reduce discretization errors. In this model, the relative tolerance is 10^{-6}, which means there is one mistake in a million results. The color legend shows magnetic flux density while the arrow represents the direction

TABLE I: Input parameters and materials used for simulations and relevant data from state-of-the-art [23, 24].

Layer	*Material*	*M_s (emu/cm^3)*	*l_{ex} (nm)*	*B_k (Oe)*
Free Layer (FL)	CoFeB	120	4.5	0.4
Barrier	MgO	-	-	-
Reference Layer (RL)	CoFeB	120	3.5	0.4
Spacer	Ru	-	-	-
Pinned Layer (PL)	CoFe	100	3	0.4
Antiferromagnet (AMF)	IrMn	-	-	-

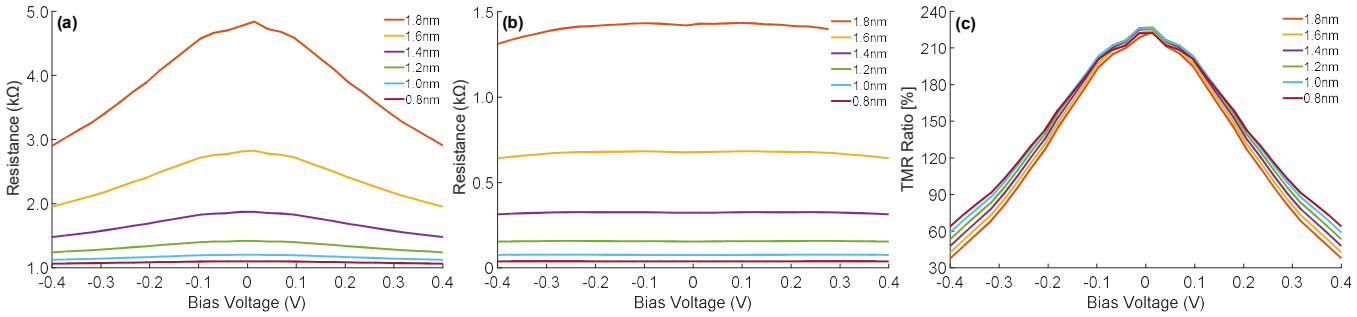

Fig. 3. Effect of t_{ox} on (a) the anti-parallel, (b) the parallel resistances of the TMR sensor and (c) on TMR ratio with different bias voltages.

of the current density.

Since the TMR sensor to be imported into *Cadence* environment with bias and AFE circuits, a magnetoresistor *Verilog-A* compact model was developed and implemented based on a physical point of view in FEM simulation results [25]. The magnetoresistor model was calculated as $R_{TMR} = R_0(1 \pm \alpha H)$, where R_0 is the initial value of resistors (Ω), α is a magnetic resistance coefficient, and H is the magnetic field ranging between [-5, +5] *Oe*. The value of α was obtained from *COMSOL* and expressed as $R_{TMR} = 3100 \cdot (1 \pm 0.00121864 \cdot H)$.

Furthermore, a full Wheatstone bridge compact model with null voltage output in expose of an external magnetic field was implemented to compensate thermal drift. The differential outputs from the bridge model are amplified by an AFE comprise of a transimpedance amplifier and a low-pass filter.

III. Simulation Results

In the MTJ, an insulator layer is sandwiched between two magnetic layers. The current flowing through the tunnelling causes the thickness (t_{ox}) of the insulator layer to have a positive effect on the output. Figure 3(a) and (b) show the variation of resistance at the parallel state and anti-parallel state with respect to the low bias voltage in the different thicknesses of the barrier. The shape of anti-parallel resistances is a semi-parabola. What stand out from these results are that: (1) the resistance of an MTJ is much higher than that in the parallel configuration, which is in accordance with the TMR mechanism of the MTJ; (2) the resistance does not reach the maximum value at zero bias due to the asymmetry of the barrier height; (3) the thickness of the barrier affects the MTJ performance significantly. At a fixed bias voltage, if the value of t_{ox} is increased then the value of R_P/R_{AP} is also increased and vice versa. In summary, if a small bias voltage is applied to the MTJ, large anti-parallel and parallel resistances can be obtained.

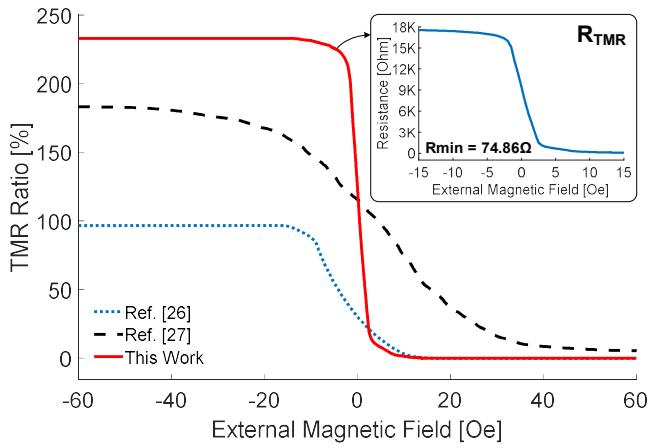

Fig. 4. TMR response compared to [26] and [27].

In addition, the voltage dependence of TMR can be seen in Fig. 3(c). The TMR is a function of the applied bias voltage, in which TMR decreases by increasing the junction voltage due to the increase of the barrier height. A group of quadratic curves is obtained with a maximum value of TMR = 233% at V_B = 10 mV and $t_{ox} = 1$ nm. Finally, the linear relationship without hysteresis between the external magnetic field and the output voltage is compared in Fig. 4. By integrating the improved electrical tunnelling model iteratively in the FEM simulation, the output voltage of the MTJ with a bias voltage of 10 mV and a barrier thickness of 1 nm is obtained. These results are consistent with previous experimental results of fabricated MTJ samples reported in the literature [10]. By comparing to other the experimental work [26, 27], our results show a higher TMR ratio and better small range linearization. In this paper, the FEM simulations have been performed at room temperature. The temperature dependence of TMR in MTJs is presented in [28, 29]. Although there exist the influences of different deposition procedures and annealing temperatures on the TMR sensor response [30], the simulation results become a reliable reference in the fabrication of certain material combinations and sensor shapes and enhance the interest of the use of a finite element software for the prediction of a model.

IV. Summary and Conclusion

We developed a compact model of a TMR sensor using FEM simulation and Verilog-A. The effect of the thickness of the insulator layer on TMR performance was presented to supportdevelopment of hybrid spintronic-CMOS magnetic sensors. A TMR ratio of 233% with 10 mV power supply was obtained from *COMSOL* and was verified *Verilog-A* model in *Cadence*. The simulation results based on MgO barrier matched well with experimental results found in the literature. The compact *Verilog-A* model in the *Cadence* environment, considering a 0.18 µm CMOS process, was implemented and verified with its AFE circuits. The high-sensitivity of TMR sensor with a linear response of an external magnetic field provides a reliable benchmark for the future development of hybrid spintronic-CMOS systems in the biomedical and neuromorphic computing applications. Special applications may be on-chip signal processing and noise and offset cancellation.

REFERENCES

[1] D. Apalkov, B. Dieny and J. M. Slaughter, "Magnetoresistive random access memory," in *Proceedings of the IEEE*, vol. 104, no. 10, pp. 1796-1830, October 2016. DOI: 10.1109/JPROC.2016.2590142

[2] L. Xu, H. Yu, M. S. Akhras, S. Han, S. Osterfeld, R. L. White, N. Pourmand, S. X. Wang, "Giant magnetoresistive biochip for DNA detection and HPV genotyping," *Biosensors and Bioelectronics*, vol. 24, iss. 1, pp. 99–103, March 2008. DOI: 10.1016/j.bios.2008.03.030.

[3] S. X. Wang and G. Li, "Advances in giant magnetoresistance biosensors with magnetic nanoparticle tags: Review and outlook," *IEEE Transactions on Magnetics*, vol. 44, no. 7, pp. 1687-1702, July 2008.DOI: 10.1109/TMAG.2008.920962

[4] D.A. Hall, R.S. Gaster, T. Lin, S.J. Osterfeld, S. Han, B. Murmann, S.X. Wang, "GMR biosensor arrays: A system perspective," *Biosensors and Bioelectronics*, vol. 25, no. 9, pp. 2051–2057, May 2010. DOI: 10.1016/j.bios.2010.01.038

[5] E. Boto, N. Holmes, J. Leggett, G. Roberts, V. Shah, S. S. Meyer, L. D. Muñoz, K. J. Mullinger, T. M. Tierney, S. Bestmann, G. R. Barnes, R. Bowtell & M. J. Brookes, "Moving magnetoencephalography towards real-world applications with a wearable system," *Nature*, vol. 555, no. 7698, p. 657, March. 2018. DOI: 10.1038/nature26147

[6] Amaral, J., Gaspar, J., Pinto, V., Costa, T., Sousa, N., Cardoso, S., & Freitas, P., "Measuring brain activity with magnetoresistive sensors integrated in micromachined probe needles," *Applied Physics A*, vol. 111, no. 2, pp. 407–412, February 2013. DOI: 10.1007/s00339-013-7621-7

[7] B. Francesca, V. Trauchessec, L. Caruso, J. Trejo-Rosillo, B. Telenczuk, E. Paul, T. Bal, A. Destexhe, C. Fermon, and M. Pannetier-Lecoeur, "Local recording of biological magnetic fields using Giant Magneto Resistance-based micro-probes," *Scientific Reports*, vol. 6, p. 39330, December 2016. DOI: 10.1038/srep39330

[8] L. Caruso, T. Wunderle, C. M. Lewis, J. Valadeiro, V. Trauchessec, J. T. Rosillo, J. P. Amaral, J. Ni, P. Jendritza, C. Fermon, S. Cardoso, P. P. Freitas, P. Fries, M. Pannetier-Lecoeur, "In vivo magnetic recording of neuronal activity," *Neuron*, vol. 95, no. 6, pp. 1283–1291, August 2017. DOI: 10.1016/j.neuron.2017.08.012

[9] J.-Y. Chen, Y.-C. Lau, J. M. D. Coey, M. Li, and J.-P. Wang, "High performance MgO-barrier magnetic tunnel junctions for flexible and wearable spintronic applications," *Scientific Reports*, vol. 7, p. 42001, February 2017. DOI: 10.1038/srep42001

[10] P. P. Freitas, R. Ferreira and S. Cardoso, "Spintronic sensors," in *Proceedings of the IEEE*, vol. 104, no. 10, pp. 1894-1918, October 2016. DOI: 10.1109/JPROC.2016.2578303

[11] Parkin, S. S., Kaiser, C., Panchula, A., Rice, P. M., Hughes, B., Samant, M., & Yang, S. H., "Giant tunnelling magnetoresistance at room temperature with MgO (100) tunnel barriers," *Nature Materials*, vol. 3, no. 12, p. 862, October 2004. DOI: 10.1038/nmat1256

[12] Cardoso, S., Leitao, D. C., Gameiro, L., Cardoso, F., Ferreira, R., Paz, E., & Freitas, P. P., "Magnetic tunnel junction sensors with pTesla sensitivity," *Microsystem Technologies*, vol. 20, no. 4–5, pp. 793–802, January 2014. DOI: 10.1007/s00542-013-2035-1

[13] P. P. Freitas, S. Cardoso, R. Ferreira, V. C. Martins, A. Guedes, F. A. Cardoso, J. Loureiro, R. Macedo, R. C. Chaves, and J. Amaral, "Optimization and integration of magnetoresistive sensors," *Spin*, vol. 1, no. 01, pp. 71–91, June 2011. DOI: 10.1142/S2010324711000070

[14] T. Costa, M. S. Piedade, J. Germano, J. Amaral and P. P. Freitas, "A neuronal signal detector for biologically generated magnetic fields," *IEEE Transactions on Instrumentation and Measurement*, vol. 63, no. 5, pp. 1171-1180, May 2014. DOI: 10.1109/TIM.2013.2296417

[15] H. Heidari, S. Zuo, A. Krasoulis, and K. Nazarpour, "CMOS Magnetic Sensors for Wearable Magnetomyography," in *Procceding International Conference of the IEEE Engineering in Medicine and Biology Society*, 2018.

[16] Z. Yin, E. Bonizzoni and H. Heidari, "Magnetoresistive Biosensors for On-Chip Detection and Localization of Paramagnetic Particles," in *IEEE Journal of Electromagnetics, RF and Microwaves in Medicine and Biology*, vol. 2, no. 3, pp. 179-185, September 2018. DOI: 10.1109/JERM.2018.2858562

[17] K. O. Htet, R. Ghannam, Q. H. Abbasi and H. Heidari, "Power Management Using Photovoltaic Cells for Implantable Devices," in *IEEE Access*, vol. 6, pp. 42156-42164, August 2018. DOI: 10.1109/ACCESS.2018.2860793

[18] M. Julliere, "Tunneling between ferromagnetic films," *Physics Letters A*, vol. 54, no. 3, pp. 225–226, September 1975. DOI: 10.1016/0375-9601(75)90174-7

[19] A. V Silva, D. C. Leitao, J. Valadeiro, J. Amaral, P. P. Freitas, and S. Cardoso, "Linearization strategies for high sensitivity magnetoresistive sensors," *European Physical Journal Applied Physics*, vol. 72, no. 1, p. 10601, October 2015. DOI: 10.1051/epjap/2015150214

[20] V. Nabaei, R. Chandrawati, and H. Heidari, "Magnetic Biosensors: Modelling and Simulation," *Biosensors and Bioelectronics*, vol. 103, no. December 2017, pp. 69–86, April 2017. DOI: 10.1016/j.bios.2017.12.023

[21] Leitao, D C, A V Silva, R Ferreira, E Paz, F L Deepack, S Cardoso, and P P Freitas, "Linear nanometric tunnel junction sensors with exchange pinned sensing layer," *Journal of Applied Physics*, vol. 115, no. 17, p. 17E526, March 2014. DOI: 10.1063/1.4869163

[22] P. Bruno and C. Chappert, "Ruderman-Kittel theory of oscillatory interlayer exchange coupling," *Physical Review B*, vol. 46, no. 1, p. 261, July 1992. DOI: 10.1103/PhysRevB.46.261

[23] S. Ana V, D. C. Leitao, Z. Huo, R. J. Macedo, R. Ferreira, E. Paz, F. L. Deepak, S. Cardoso, and P. P. Freitas, "Switching field variation in MgO magnetic tunnel junction nanopillars: Experimental results and micromagnetic simulations," *IEEE Transactions on Magnetics*, vol. 49, no. 7, pp. 4405-4408, July 2013. DOI: 10.1109/TMAG.2013.2252330.

[24] Z. Hou, A. V Silva, D. C. Leitao, R. Ferreira, S. Cardoso, and P. P. Freitas, "Micromagnetic and magneto-transport simulations of nanodevices based on MgO tunnel junctions for memory and sensing applications," *Physica B: Condensed Matter*, vol. 435, pp. 163–167, February 2014. DOI: 10.1016/j.physb.2013.09.039

[25] H. Heidari, N. Wacker, S. Roy and R. Dahiya, "Towards bendable CMOS magnetic sensors," in *Proc. 11th Conference on Ph.D. Research in Microelectronics and Electronics (PRIME)*, pp. 314-317, 29 June–2 July 2015. DOI: 10.1109/PRIME.2015.7251398

[26] A. José, V. Pinto, T. Costa, J. Gaspar, R. Ferreira, E. Paz, S. Cardoso, and P. P. Freitas, " Integration of TMR sensors in silicon microneedles for magnetic measurements of neurons," *IEEE Transactions on Magnetics*, vol. 49, no. 7, pp. 3512-3515, July 2013. DOI: 10.1109/TMAG.2013.2239274

[27] E. Paz, R. Ferreira and P. P. Freitas, "Linearization of magnetic sensors with a weakly pinned free-layer MTJ stack using a three-step annealing process," *IEEE Transactions on Magnetics*, vol. 52, no. 7, pp. 1-4, July 2016. DOI: 10.1109/TMAG.2016.2525772

[28] J. H. Lee, K. I. Lee, W. L. Lee, K.-H. Shin, J. S. Lee, K. Rhie, and B. C. Lee, "Temperature dependence of tunneling magnetoresistance: Double-barrier versus single-barrier junctions," *Journal of applied physics*, vol. 91, no. 10, pp. 7956–7958, May 2002. DOI: 10.1063/1.1452232

[29] L. Yuan, S.-H. Liou, and D. Wang, "Temperature dependence of magnetoresistance in magnetic tunnel junctions with different free layer structures," *Physical Review B*, vol. 73, no. 13, p. 134403, April 2006. DOI: 10.1103/PhysRevB.73.134403

[30] P. J. Chen, M. Zhu, S. Tibus, T. Dyer, J. Piccirillo, B. Ocker, and R. D. Shull, "Annealing stability study of Co20Fe60B20\MgO\Co20Fe60B20 perpendicular magnetic tunnel junctions," *Journal of Physics D: Applied Physics*, vol. 50, no. 2, p. 25006, December 2016. DOI: 10.1088/1361-6463/50/2/025006